Naval Research Laboratory

Washington, DC 20375-5320

NRL/MR/5917-93-7303

ELASTIC MODULI OF ALUMINUM-POLYURETHANE COMPOSITES (ALUMERS)

Pieter S. Dubbelday

Naval Research Laboratory
Underwater Sound Reference Detachment
P.O. Box 568337, Orlando, FL 32857-8337

15 May 1993

Approved for public release; distribution unlimited.

REPORT DOCUMENTATION PAGE

Form Approved
OMB No. 0704-0188

1. AGENCY USE ONLY (Leave blank)	2. REPORT DATE	3. REPORT TYPE AND DATES COVERED
	15 May 1993	FINAL

4. TITLE AND SUBTITLE
Elastic Moduli of Aluminum-polyurethane Composites (Alumers)

5. FUNDING NUMBERS
PE - 61153N
TA - RR011-08-42
WU - DN280-003

6. AUTHOR(S)
Dr. Pieter S. Dubbelday

7. PERFORMING ORGANIZATION NAME(S) AND ADDRESS(ES)
NAVAL RESEARCH LABORATORY
UNDERWATER SOUND REFERENCE DETACHMENT
P.O. BOX 568337
ORLANDO, FL 32856-8337

8. PERFORMING ORGANIZATION REPORT NUMBER
NRL Memorandum Report 7303

9. SPONSORING/MONITORING AGENCY NAME(S) AND ADDRESS(ES)
OFFICE OF NAVAL RESEARCH
800 N. QUINCY STREET
ARLINGTON, VA 22217-5000

10. SPONSORING/MONITORING AGENCY REPORT NUMBER

11. SUPPLEMENTARY NOTES

12a. DISTRIBUTION/AVAILABILITY STATEMENT
Approved for public release; distribution unlimited.

12b. DISTRIBUTION CODE
A

13. ABSTRACT (Maximum 200 words)

In this report, results are given of the bulk modulus measurement of some selected polyurethanes and of the bulk and Young's modulus of these polyurethanes and composites. These composites consist of a matrix of foamed aluminum impregnated with the various polymers. The composites are named "alumers", a contraction of "aluminum" and "elastomer". These materials are designed to be approximately transparent to sound, since both density and sound speed are close to those for the medium, in this case (sea)water. The foamed aluminum matrix supplies mechanical strength for those applications where the material is used for structural support.

14. SUBJECT TERMS
Rigid rho-c material; composite; elastic moduli; Young's modulus; bulk modulus

15. NUMBER OF PAGES
47

16. PRICE CODE

17. SECURITY CLASSIFICATION OF REPORT	18. SECURITY CLASSIFICATION OF THIS PAGE	19. SECURITY CLASSIFICATION OF ABSTRACT	20. LIMITATION OF ABSTRACT
UNCLASSIFIED	UNCLASSIFIED	UNCLASSIFIED	UL

BLANK PAGE

CONTENTS

BLANK PAGE

ELASTIC MODULI OF ALUMINUM-POLYURETHANE COMPOSITES (ALUMERS)

INTRODUCTION

In acoustical design, it is often desirable to have an acoustically transparent material available; i.e., a material with density ρ (rho) and dilatational speed c_d that closely match the density and compressional wave speed in the medium, usually (sea)water. This ideal may be closely approached by elastomers in the rubbery state. These are sometimes called "rho-c rubber" (a trade name of B.F. Goodrich). The shear modulus G of these elastomers is low and, as a consequence, they do not offer the structural support that may be needed in some applications.

A rigid, acoustically transparent material, based on a fluoroepoxy matrix into which glass and phenol microballoons are dispersed, has been described in the literature [1]. In this report a different composite, aimed at obtaining the desired match, is introduced; it consists of a foamed aluminum matrix, impregnated with a two-part polyurethane [2]. The term "alumer" (a contraction of aluminum and elastomer) is proposed for these composites.

It may be noted here that a solid material necessarily deviates from ideal acoustic transparency by virtue of the presence of a finite shear modulus, causing reflections at other than normal incidence--even with perfectly matched ρ and c_d [3]. This effect is particularly important near grazing incidence and near thickness-shear resonances.

In interpreting the experiments, it is assumed that, at low frequency, the composite behaves as a homogeneous, isotropic material, characterized by two

Manuscript approved 15 March 1993

independent complex moduli (one of the constituents, the foamed aluminum, shows anisotropic behavior; it is assumed that this does not make a noticeable difference in the composite). One may compare this situation with the case of fluid-filled, porous materials where Biot's theory predicts the presence of three waves: two in the solid and one in the fluid. The coupling between the two solids encountered in this study demands continuity of both the normal and the tangential stress; as a consequence, it would be difficult to imagine independent waves propagating in the two solid constituents. There was no literature found that deals with this possibility.

This report discusses the measurement of the bulk modulus of pure polyurethanes and the corresponding alumers. Possible systematic errors in the measurement of Young's modulus are discussed, and a correction model is presented. The results of the measurement of Young's modulus E of the alumers are given (the Young's modulus of the polyurethanes is taken from the literature). The dilatational wave speed is computed, and the resulting ρc-products are listed.

BULK MODULUS OF ELASTOMERS

In Fig. 1, the results of a complex bulk modulus K^* measurement as a function of frequency are shown for (soft) natural rubber AA165-4 (see Ref. 4 for a discussion of the measurement method). The modulus is expressed in terms of real and imaginary parts by $K^* = K' + iK''$; the loss tangent is $\tan \delta_K = K''/K'$. Only the solid parts of the curves are considered to represent true values for K' and $\tan \delta_K$. One sees that at higher frequencies the curve for K' (dashed part) turns down; this is due to the fundamental chamber resonance at about 8 kHz. For this reason and because of another structure visible in most other cases (see below), the validity of the data is assumed to be limited to values between 50 and 500 Hz. The pressure in the measurement coupler is 2.5 MPa throughout.

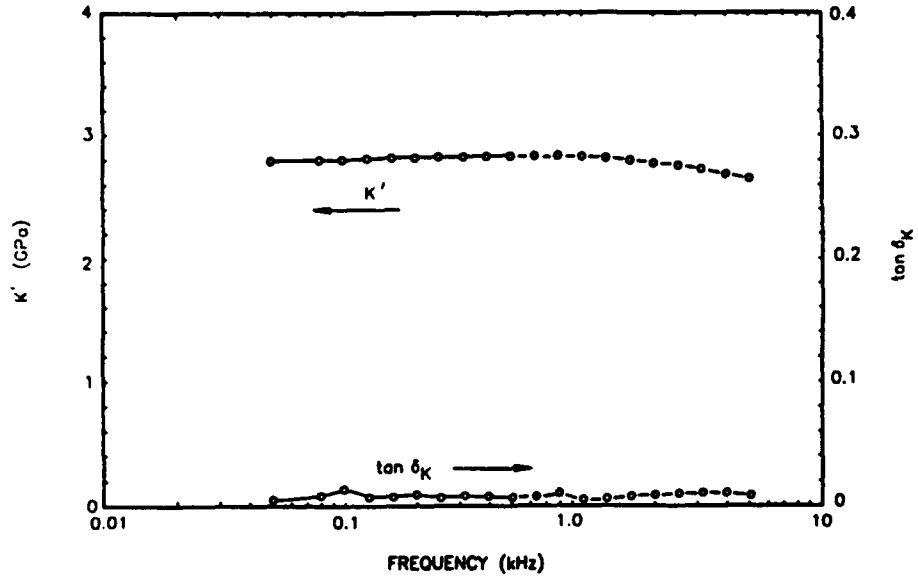

Fig. 1. Results of the data reduction of the dynamic bulk modulus measurement as a function of frequency at 8°C for natural rubber AA165-4 (aged 5 years in seawater). The solid parts of the curves (connecting the measured points) are considered to be the real part K' and the loss tangent tan δ_K of the bulk modulus; the dashed parts are affected by the chamber resonance.

One expects that the bulk modulus will show viscoelastic behavior in its dependence on frequency and temperature, although less so than the Young's or shear modulus. In Refs. 4 and 5 this viscoelastic behavior is analyzed for some specific elastomers for which the frequency and temperature dependence of K' and tan δ_K showed the familiar viscoelastic structure. In the present study this is not pursued further; instead, an average is given in the tables for K' and tan δ_K over the frequency range of 50 to 500 Hz.

As an indication of the error involved, the standard deviation of the population is given, estimated from the variation in the values over the given frequency range, in order to account for a possible systematic frequency dependence; a large value of this error is generally connected with a trend visible in the graphs. For mutual comparison of the experimental K' values, this is an adequate measure of uncertainty. Since the method relates the values of K' to the bulk modulus of castor oil, the absolute value of K' may be

subject to a systematic error of about 2% due to the accuracy limit in the compressibility of castor oil [6].

BULK MODULUS OF POLYURETHANES

Figure 2 shows the values for K' at 10, 20, and 30°C for the four polyurethanes that were used as components of the alumers; PR 1526, PR 1538, PR 1574, and PR 1590. The PR designation is given by the company that produces these elastomers, Polymer Research Co. These four elastomers were chosen based on their stiffness at room temperature and at a frequency near 1000 Hz; PR 1526 is soft, PR 1574 is hard, and the other two are in between. A description of their general and physical properties may be found in Ref. 7.

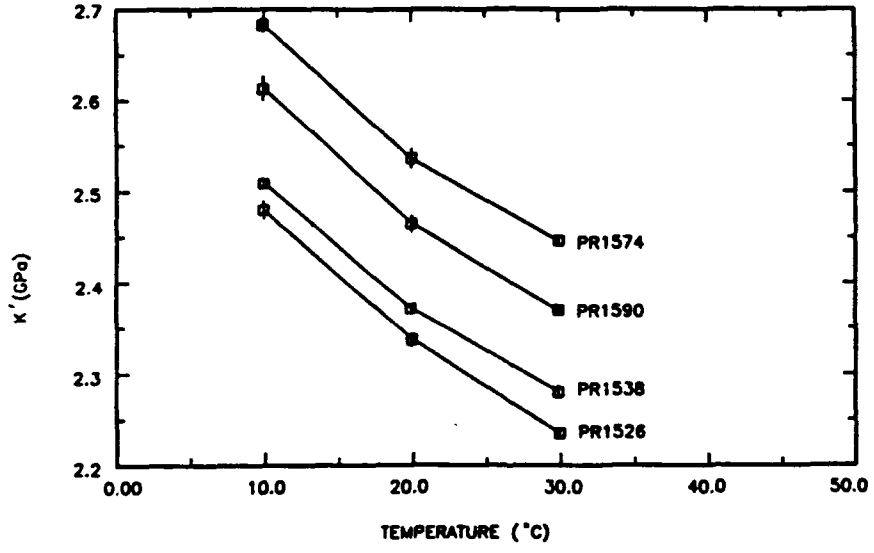

Fig. 2. Real part of the bulk modulus K' averaged from 50 to 500 Hz as a function of temperature for four polyurethanes. The solid lines connect the points at 10, 20, and 30°C. The error bars at the measurement points represent the standard deviation of the population (estimated from the variation with frequency) at that temperature.

The solid curves were drawn to guide the eye. At each measurement point, the error bar represents the standard deviation for the population, from the average over the frequency range from 50 to 500 Hz. One can see a similar dependence on temperature for each of the four curves. The values of the bulk modulus for the four elastomers at a given temperature vary little, no more than by about 0.2 GPa, as is typical for elastomers. In contrast, the values for Young's modulus vary considerably (see the relevant section below).

In Fig.3 the values for tan δ_K are given for the same polyurethanes with the same parameters. The error limits are not depicted, since the overlap would result in a confusing picture. The standard deviation in tan δ_K is typically 0.004; a larger value generally corresponds to a noticeable trend in the data as a function of frequency.

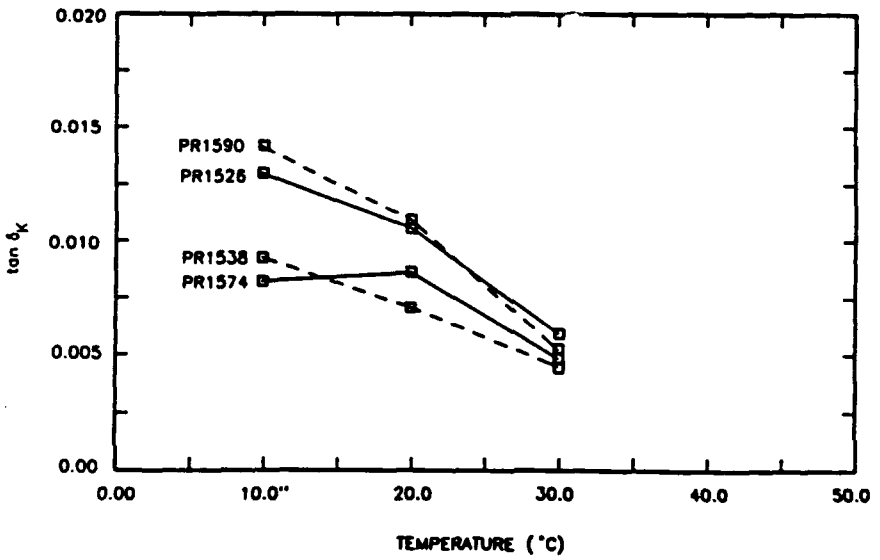

Fig. 3. Loss tangent tan δ_K of the bulk modulus averaged from 50 to 500 Hz as a function of temperature for four polyurethanes. The lines connect the points at 10, 20, and 30°C.

BULK MODULUS OF ALUMERS

Table 1 shows the results for the values of K' and tan δ_K, at three temperatures, for the pure polyurethanes and the alumer types based on these elastomers when combined with foamed aluminum of 6% nominal density and pore sizes of 10, 20, and 40 pores per inch (ppi). The errors given are estimates of the standard deviations for the population obtained by averaging over the frequency range.

Table 1. Values for the real part of the bulk modulus K' and the loss tangent tan δ_K for pure polyurethanes.

Elastomer type	Pore size of foam, ppi		Temperature, °C		
			30	20	10
PR 1526	elastomer only	K', GPa	2.236±0.002	2.337±0.007	2.481±0.009
		tan δ_K	0.006±0.005	0.011±0.002	0.013±0.001
	10	K', GPa	2.486±0.007	2.601±0.010	2.747±0.010
		tan δ_K	0.011±0.002	0.016±0.002	0.018±0.002
	20	K', GPa	2.520±0.008	2.651±0.011	2.846±0.009
		tan δ_K	0.012±0.003	0.016±0.002	0.016±0.003
	40	K', GPa	2.556±0.006	2.654±0.008	2.836±0.007
		tan δ_K	0.007±0.003	0.011±0.002	0.014±0.003
PR 1538	elastomer only	K', GPa	2.28[illegible]±0.005	2.371±0.003	2.511±0.004
		tan δ_K	0.004±0.004	0.007±0.003	0.009±0.003
	10	K', GPa	2.543±0.008	2.662±0.011	2.712±0.029
		tan δ_K	0.007±0.003	0.011±0.001	0.035±0.007
	20	K', GPa	2.468±0.010	2.568±0.017	2.744±0.017
		tan δ_K	0.010±0.004	0.017±0.003	0.022±0.003
	40	K', GPa	2.491±0.007	2.610±0.005	2.662±0.031
		tan δ_K	0.011±0.002	0.012±0.003	0.036±0.002
PR 1574	elastomer only	K', GPa	2.446±0.005	2.537±0.010	2.683±0.006
		tan δ_K	0.005±0.005	0.008±0.002	0.008±0.001
	10	K', GPa	2.824±0.011	2.938±0.016	3.053±0.020
		tan δ_K	0.006±0.002	0.004±0.002	0.005±0.004
	20	K', GPa	2.842±0.018	2.962±0.017	3.076±0.019
		tan δ_K	0.003±0.003	0.003±0.001	0.003±0.002
	40	K', GPa	2.852±0.010	2.974±0.015	3.116±0.009
		tan δ_K	0.007±0.003	0.010±0.003	0.010±0.002
PR 1590	elastomer only	K', GPa	2.369±0.004	2.466±0.009	2.614±0.012
		tan δ_K	0.005±0.005	0.011±0.004	0.014±0.002
	10	K', GPa	2.555±0.006	2.713±0.016	2.848±0.002
		tan δ_K	0.011±0.004	0.016±0.004	0.025±0.003
	20	K', GPa	2.608±0.006	2.753±0.009	2.877±0.014
		tan δ_K	0.008±0.003	0.014±0.003	0.026±0.004
	40	K', GPa	2.621±0.009	2.736±0.013	2.911±0.032

To evaluate the influence of the aluminum matrix on the effective bulk modulus in the alumers, one may study the ratio of K_p'/K_a', where the numerator is the bulk modulus of the pure polymer material and the denominator the bulk modulus of the given alumer. The results are shown in Table 2. In addition to the results at a given temperature and pore size, averages are shown for alumers with given pore size and different temperatures and for different pore sizes at a stated temperature.

The results in Table 2 show that the variations with pore size and temperature of K' for a given filler appear generally insignificant, except for the alumers based on PR 1538 with 10 ppi and 40 ppi foamed aluminum at 10 °C, for which the K' is significantly larger than at the two higher temperatures. If one looks at the average over all the data for an alumer based on a given polymer, one sees a gradual increase of the ratios in the following order, from low to high: PR 1574, 0.864; PR 1526, 0.886; PR 1590, 0.908; PR 1538, 0.916.

One may give the following interpretation of the data in Table 2, when averaged for each of the four groups. Ignoring the (small) compliance of the aluminum in the matrix, one could approximate the compliance of the composite by that of the polymer, assumed not to be influenced by the matrix, equal to the porosity of the foamed aluminum ϕ multiplied by the inverse bulk modulus of the elastomer. Thus $K'_p/K'_a \simeq (V_p\ \beta_p)/[\beta_p(V_a+V_p)] = \phi$, where V_p is the volume of the polymer in the composite, V_a the volume of the foamed aluminum, and β_p the specific compliance of the pure polymer.

As a consequence, one would expect that the above ratio of moduli would be approximately equal to the porosity of the foamed aluminum, nominally equal to 0.94. The fact that the ratios are smaller than this number indicates that the aluminum matrix decreases the compliance of the polymer filler.

Table 2. Ratio of the bulk modulus for the pure polyurethane and the bulk modulus of the alumer based on that polyurethane.

Elastomer type	Pore size of foam, ppi	Temperature, °C				
		30	20	10	Average, pore size	Average, alumer
PR 1526	10	0.900	0.899	0.903	0.901	
	20	0.887	0.882	0.872	0.880	
	40	0.875	0.881	0.875	0.877	
	Average for temperature	0.887	0.887	0.883		0.886
PR 1538	10	0.897	0.891	0.926	0.905	
	20	0.925	0.923	0.915	0.921	
	40	0.916	0.908	0.943	0.922	
	Average for temperature	0.913	0.907	0.928		0.916
PR 1574	10	0.866	0.863	0.879	0.869	
	20	0.860	0.856	0.872	0.865	
	40	0.858	0.853	0.861	0.857	
	Average for temperature	0.861	0.857	0.871		0.864
PR 1590	10	0.927	0.910	0.918	0.918	
	20	0.908	0.896	0.909	0.904	
	40	0.904	0.901	0.898	0.901	
	Average for temperature	0.913	0.902	0.908		0.908

In the literature, one finds models that are designed to relate the bulk and shear modulus of a composite to the properties of the components. The model of Van der Poel [8] (also found in Christensen [9]) was applied here. The values found are considerably farther removed from the measured values than those that follow from the compliance of the polymer, as given above. For instance, in the case of the alumer consisting of 6% relative density aluminum and PR 1574 filler at 30°C, the value of K', according to Van der Poel's model, is 3.9 GPa, about 50% larger than the experimental value. The experimental values for K' show no clear correlation with the shear modulus; this would appear to confirm the result of Van der Poel's model, namely, that the effective K' depends only on the shear modulus of the matrix, and not on that of the filler. None of the models found in the literature account for the pore size of the matrix, only for its porosity. Temperature does not enter explicitly, since the model uses the values of K' of the two constituents at a given temperature. The models are developed for the steady state, but the results for the bulk modulus should not be noticeably different from those at low frequency.

The values for the loss tangent tan δ_K (Table 1) show some systematic effects. The standard deviation of the population varies from about 0.001 to 0.004. The larger values usually reflect a trend that is visible in the graphs.

For the pure polyurethanes at 10 and 20°C, the values of tan δ_K for PR-1590 and PR-1526 are close, so are the other two (see Fig. 3). At 30°C all four moduli come close together. In almost all cases, tan δ_K of the composite is higher than that of the elastomer by not more than a factor of about 2. An exception is found in the alumers based on PR 1538; at 10°C the loss tangent is up to a factor of four larger for the alumers than for the pure elastomer at the three pore sizes.

STRUCTURE IN THE GRAPHS FOR BULK MODULUS AND LOSS TANGENT

Figure 1 is an example of a favorable case in that the smooth appearance of the curve shows the variation of modulus and loss tangent with frequency below the chamber resonance. For the majority of other polymers a structure appears in the K' and tan δ_K curves, as illustrated by Fig. 4, which shows these quantities for a sample of PR 1538 at three temperatures. The structure is even more pronounced for a hard elastomer like PR 1574, shown in Fig. 5, and it is found for all the alumers that have been investigated.

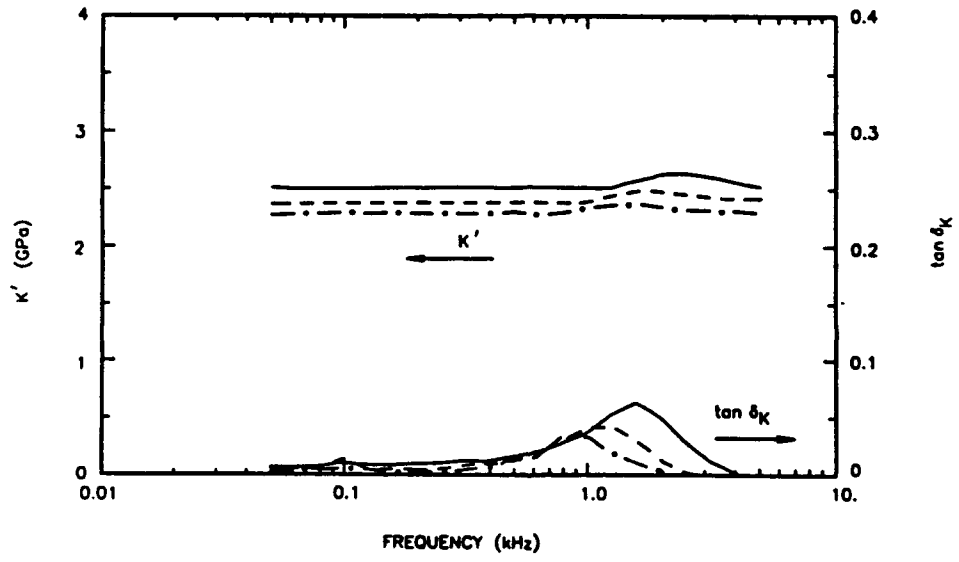

Fig. 4. Results of the data reduction of the bulk modulus measurement for PR 1538 as a function of frequency at three temperatures. The data above 500 Hz are not considered to represent the dynamic bulk modulus, since they are affected by consequences of the experimental method. Solid curve, 10 °C; dashed curve, 20°C; dotted-dashed curve, 30°C.

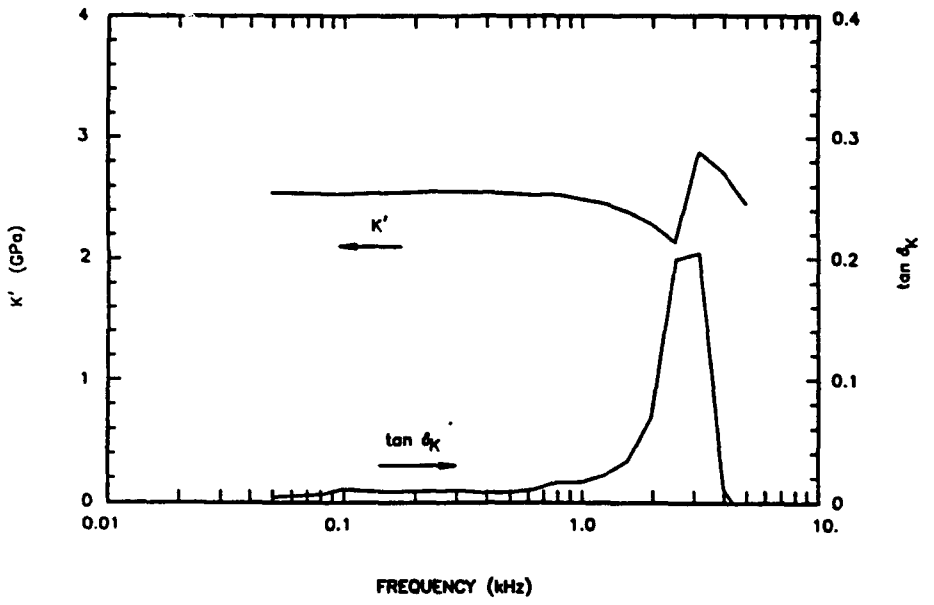

Fig. 5. Results of the data reduction of the bulk modulus measurement for PR 1574 as a function of frequency at 25°C. The data above 500 Hz are not considered to represent the dynamic bulk modulus, since they are affected by consequences of the experimental method.

At one time, it was thought that this structure might be related to relaxation in the material at hand. The following arguments are contrary to this notion:

1. The width of the loss peak is much narrower than would correspond to a single relaxation time, while the viscoelastic phenomena are always related to a broad spectrum of relaxation times.
2. The structure shifts to lower frequencies when the temperature is decreased; this is opposite to the temperature-frequency shift known in viscoelastic behavior.

The most probable cause for this structure is the presence of a bar-type resonance in the (cylindrical) sample. Under this assumption, the resonance frequency would scale according to $c_E/\ell = \sqrt{(E/\rho)}/\ell$, where c_E is the bar speed, ℓ the length of the cylinder, and ρ the density of the material. It was found for a sample of PR 1574 that the resonance frequency shifted upward by a

factor very close to 1.5 when the cylinder length was reduced to 2/3 of its original length, confirming the assumed length dependence. The structure disappeared completely out of the given frequency range when the cylinder was replaced by a sphere equal in diameter to the cylinder. On the other hand, the shift of the resonance frequency did not appear to follow the $\sqrt{E}$ dependence. Despite this failure to follow the $\sqrt{E}$ dependence, the basic cause is still thought to be a bar resonance. One can easily advance arguments why deviations from a simple bar resonance would occur: the cylinder is loaded by the castor oil fill-fluid and the space between the cylinder and the chamber is quite narrow, such that viscosity and flow about the cylinder might play a role.

In summary, these arguments lead to the conclusion that the observed structure is not due to an effect of molecular processes on the bulk modulus. In order to avoid interference of the observed feature with the stated measurement values, the averaging of K' and $\tan \delta_K$ described before was limited to the range of 50 to 500 Hz, where this type of structure was not visible in any of the samples investigated. Some remaining deviations from a smooth curve, such as the single-measurement point at 0.1 kHz in Fig. 4, are considered to be spurious.

ELASTIC PROPERTIES OF FOAMED ALUMINUM

The measurement of Young's modulus and Poisson's ratio of various types of foamed aluminum is described in Ref. 10. The relevant properties are given here (Table 3) in order to assess the way in which these properties enter into the composite alumer. The Young's modulus measurement consists of observing the complex ratio of the accelerations, or velocities, of the base and the tip of a bar as a function of frequency, and finding the dimensionless wave number for extensional waves by means of a complex root finder [11]. In the study reported in Ref. 10, the velocities were measured by means of a laser Doppler vibrometer; for the measurement of the Young's modulus of the alumers, discussed below, accelerometers were used to determine the accelerations. The latter arrangement is similar to the one described in Ref. 7, which was used to determine Young's modulus of the pure polyurethanes.

Table 3 - Elastic properties of foamed aluminum; ppi - pores per inch; E - Young's modulus; ν - Poisson's ratio; ρ - density; ϕ - porosity; K - bulk modulus.

ppi	E (MPa)	ν	ρ kg/m^3	ϕ	K (MPa)	Dilat. modulus (MPa)	Dilat. speed (m/s)
	Nominal relative density 6%.						
10	$1/s_{11}$ = 207	0.33 = $-s_{13}/s_{11}$	177	0.93		-	-
20	$1/s_{33}$ = 194	0.42 = $-s_{13}/s_{33}$	160	0.94	120	c_{11}=194	1053
	$1/s_{11}$ = 157	0.26 = $-s_{13}/s_{11}$	175	0.935		c_{33}=248	1190
		0.23 = $-s_{12}/s_{11}$					
40	174	0.332	161	0.94	173	260	1271
	Nominal relative density 12%.						
10	$1/s_{11}$ = 236	0.24 = $-s_{13}/s_{11}$	258	0.904	-	-	-
20	$1/s_{11}$ = 311	0.19 = $-s_{13}/s_{11}$	275	0.898	-	-	-
		0.27 = $-s_{12}/s_{11}$					
40	251	0.22	281	0.896	149	287	1011

In Ref. 10, it was mentioned that some of the foamed aluminum samples did not appear to be isotropic to visual inspection. An attempt was made to explain the measurements in terms of the set of compliances that correspond to uniaxial symmetry. Stiffness and compliance matrices are given in Appendix A. Where applicable, Young's moduli and Poisson's ratios in Table 3 are expressed in terms of the compliances s_{ij}. Only in some of the cases was there sufficient information to compute the dilatational speed in the foamed aluminum.

The values for Young's modulus of foamed aluminum reported in Ref. 10 may be compared with a quadratic dependence of the modulus on the relative density of the foam, as described by Friis et al.[12] and Warren and Kraynik [13] (these authors also give theoretical expressions for Poisson's ratio). Warren and Kraynik present a justification for this functional dependence by a model based on a tetrahedral unit cell, which contains four identical half-struts joined at equal angles. For low-density foams the Young's modulus E, relative to the modulus of the solid material E_o, is given by

$$\frac{E}{E_o} = C\,\rho_r^2 \qquad (1)$$

where ρ_r is the relative density and C is a constant that depends on the assumed strut geometry: C = 0.91 for circular cross section, 1.10 for triangular cross section, and 1.53 for a Plateau border (the space between three identical, mutually tangent circles, typical for liquid foams of very thin films).

Figure 6 shows the values for E given in Table 3 as a function of relative density ρ_r with three curves according to Eq.(1), with C = 0.667, 1.00, and 1.35. The value of 0.67 for C gives reasonable agreement between the theoretical curve and the measurement points, at least for the points of nominal relative density of 6%.

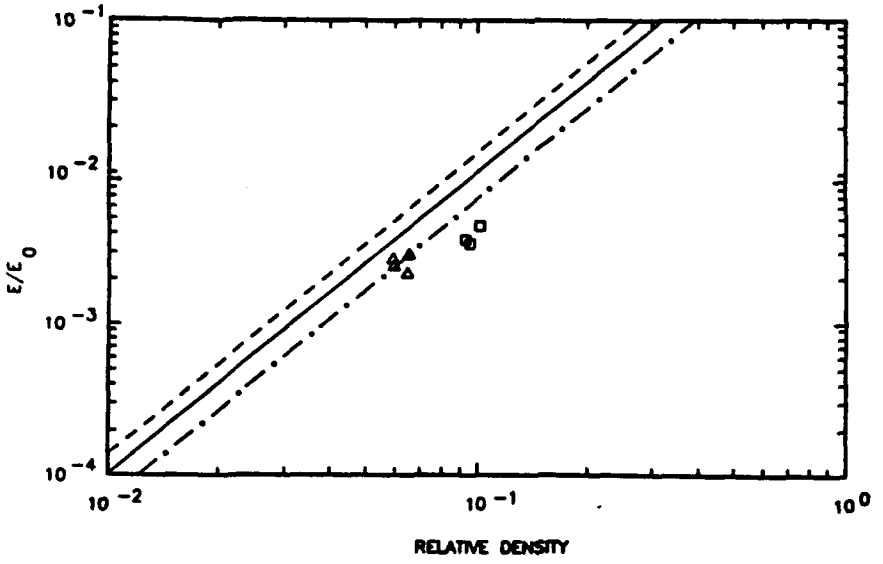

Fig. 6. Measured values of Young's modulus E for foamed aluminum, relative to the modulus of the solid material E_o, as a function of relative density ρ_r, compared with a quadratic model $E/E_o = C\,\rho_r^2$ (Warren and Kraynik [11]), where ρ_r is the relative density and C a constant that depends on the assumed strand cross section. Solid line, C = 1.; dashed line, C = 1.35; dotted-dashed line, C = 0.67. Nominal relative density: triangles, 6%; squares, 12%.

Warren and Kraynik discuss another model based on a cubic unit cell. The resulting dependence of E is linear in ρ_r. This fits the slope of the experimental points better, but the numerical values are off by an order of magnitude.

YOUNG'S MODULUS FOR PURE POLYURETHANES

Figure 7 shows the real part E' of Young's modulus as a function of frequency for the four polyurethanes used in this study at 22°C temperature. The loss tangent of these polymers is given in Fig. 8. These graphs were computed from the polynomial coefficients given by Capps [7]. One sees that PR 1526 is soft and has the largest loss tangent, PR 1538 and PR 1590 have comparable E', and PR 1574 is considerably harder.

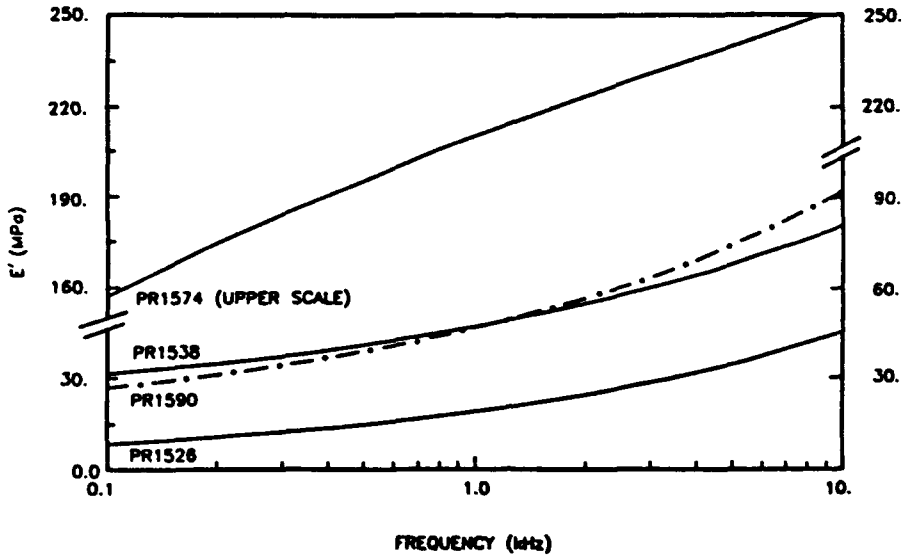

Fig. 7. Real part of Young's modulus E' as a function of frequency at 22°C for four polyurethanes, computed from polynomial coefficients in Capps [7].

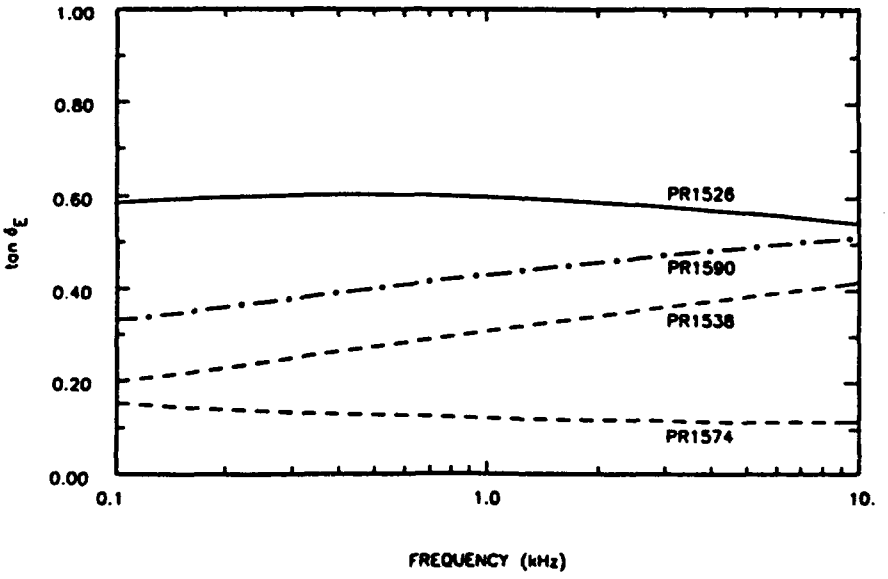

Fig. 8. Loss tangent of Young's modulus tan δ_E as a function of frequency at 22°C for four polyurethanes, computed from polynomial coefficients in Capps [7].

SYSTEMATIC ERRORS IN YOUNG'S MODULUS MEASUREMENT

The measurement of Young's modulus of the alumers was performed without the benefit of an environmental chamber, at room temperature which, of course, fluctuates and is a source of systematic error in the data.

By deliberately changing the temperature of the room, it was possible to obtain an estimate of the effect of the temperature fluctuations. The value of E' decreases for increasing temperature, concurrent with viscoelastic behavior, but the shift is larger than expected on the basis of the temperature effect computed from the information in Ref. 7. The change in the loss tangent is comparable to that of the pure elastomer according to Ref. 7.

In the listing of the data below it will be assumed that the nominal temperature is 22°C. The temperature fluctuations are estimated to result in an uncertainty in E' of ±6 MPa and ±0.006 in tan δ_E.

In almost all of the results for the real part and loss tangent of Young's modulus, one notices a structure at regular intervals. A typical example is found in the reduced data for the pure polyurethane PR 1574, Figs. 9 and 10. While investigating this effect, it was found that other modes of bar vibration, like flexural and torsional modes, did not appear to cause these measurement problems. The features shown in Figs. 9 and 10 appear near values of $k\ell$ (k is the complex wavenumber), for which the absolute ratio of the accelerations of base and tip is maximum. A possible cause for this effect is derived as follows.

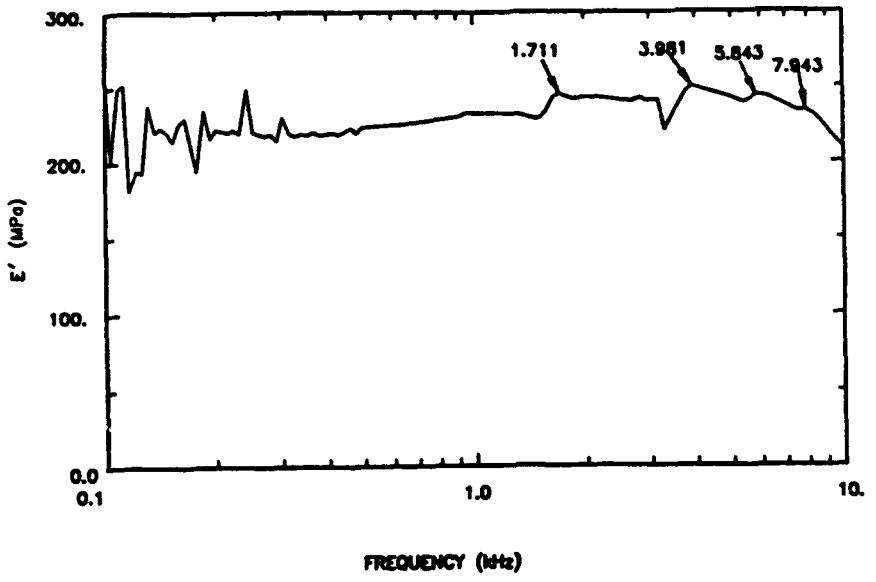

Fig. 9. Results of the data reduction for the real part of Young's modulus E' of PR 1574 polyurethane at 22°C as a function of frequency. The deviations from a smooth, monotonic curve are assumed to be due to experimental effects discussed in the text.

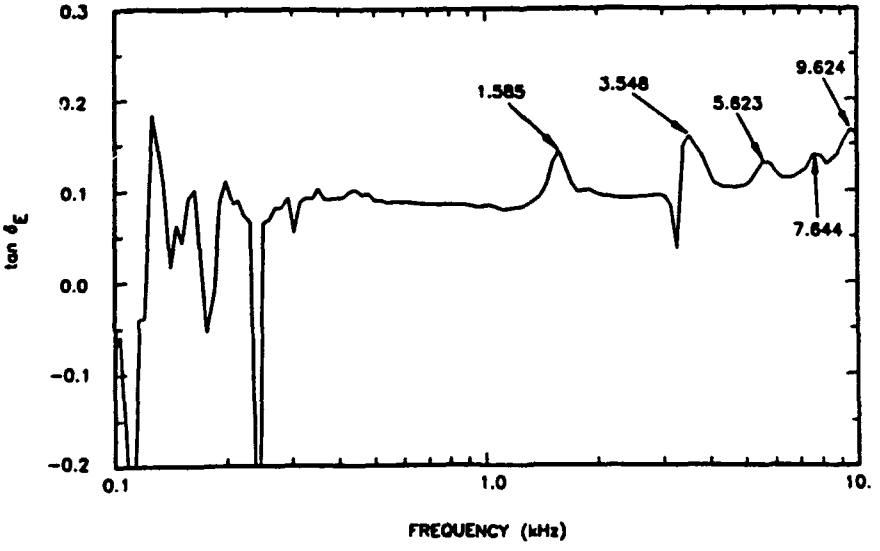

Fig. 10. Results of the data reduction for the loss tangent tan δ_E of Young's modulus of PR 1574 polyurethane as a function of frequency. The deviations from a smooth curve are assumed to be due to experimental effects discussed in the text.

The observation equation for the reduction of the data is given by

$$R = \cos z - r z \sin z, \tag{2}$$

where R is the complex ratio of the acceleration (velocity or displacement) of the base to that of the tip of the bar; and z is the complex dimensionless wavenumber, $z = k\ell$. The symbol r represents the ratio of the masses of tip and bar, $r = m_3 / m_2$. By approximating the errors in z and R, Δz and ΔR, by the first term in a Taylor series expansion, one can relate the relative errors by

$$\frac{\Delta z}{z} \simeq - \frac{\cos z - rz \sin z}{z \sin z\,(1+r) + r z^2 \cos z} \frac{\Delta R}{R.} \tag{3}$$

This expression shows that near a maximum of R the numerator is finite, while the denominator goes to zero. (To simplify the argument it is assumed that the loss tangent is zero. For complex values of R and z with small loss tangents, the thrust of the derivation remains valid). Thus near maxima of R one finds a considerable amplification factor resulting in a large relative error for $k\ell$ given a moderate relative error in R (see Pritz [14]; Capps [7] gives references to other error analyses). On the other hand, for values of z where R is close to zero, the resulting error in z goes to zero. For a small loss factor the relative error in E' is the negative of twice the relative error in z, and thus for complex R and z, one has

$$\frac{\Delta E}{E} \simeq \frac{\cos z - rz \sin z}{(1+r)z \sin z + r z^2 \cos z}\, 2 \frac{\Delta R}{R.} \tag{4}$$

Analyzing the expression on the left side of this equation in terms of the real part of Young's modulus E' and loss tangent $\tan \delta_E$, one finds that for a small loss factor the relative error in E' and the error in $\tan \delta_E$ are approximately given by

$$\frac{\Delta E'}{E'} \simeq \mathrm{Re}\, \frac{\Delta E}{E} \tag{5}$$

and

$$\Delta(\tan \delta_E) \simeq \mathrm{Im}\, \frac{\Delta E}{E}, \tag{6}$$

where Re and Im indicate the real and imaginary parts of a complex quantity.

One notices also that for $z \to 0$ the error in E' increases beyond bounds. This causes the random error to fluctuate more extensively at low frequency; in some cases where the random error is small, one finds a corresponding systematic deviation in E'.

Figures 11 and 12 show the computed behavior of the errors in E' and tan δ_E for a 1% error in R, as a function of frequency, for the above example of pure PR 1574 polyurethane. The errors have the location and appearance of the structure in the reduced data from the experiment (Figs. 9 and 10).

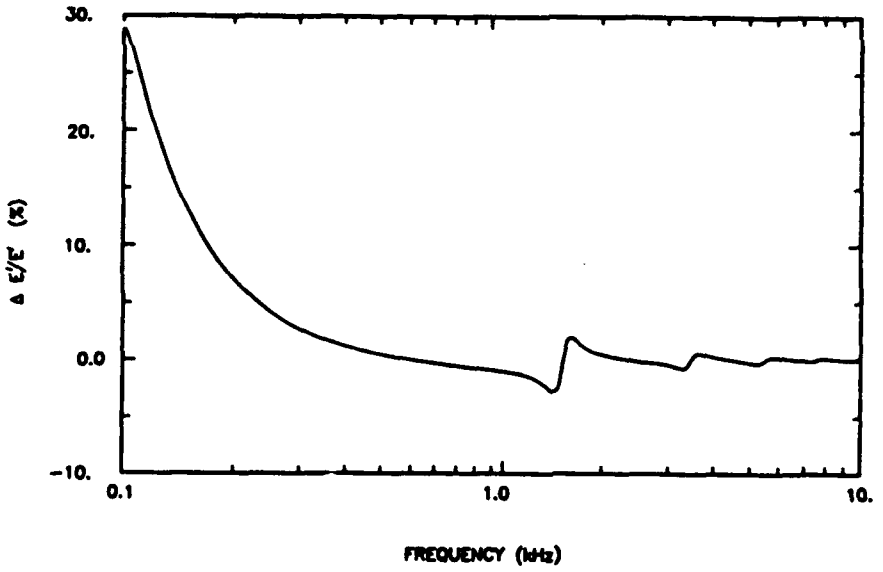

Fig. 11. Computed percentage error $\Delta E'/E'$ in the real part of Young's modulus E' for a 1% error in the ratio R of the accelerations of base and tip of the bar for polyurethane 1574

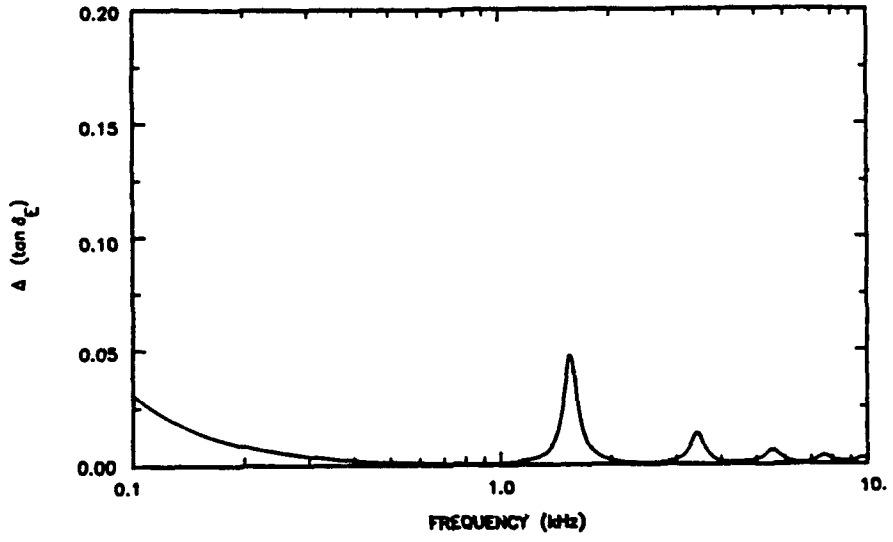

Fig. 12. Computed error Δ (tan δ_E) in the loss tangent tan δ_E of Young's modulus for a 1% error in the ratio R of the accelerations of base and tip of the bar for polyurethane PR 1574

Figure 13 shows the effect on tan δ_E of correcting the data near the first occurring structure by applying percentage changes in R. A value of -1.4% appears to reduce the systematic deviation to a random fluctuation. Even a small variation of the relative error produces a noticeable deviation. The corresponding effect of this -1.4% correction in R on E' is shown in Fig.14. This same correction of -1.4% carried through the higher frequency range does not give smoother curves for E' nor for tan δ_E for the structures at higher frequency.

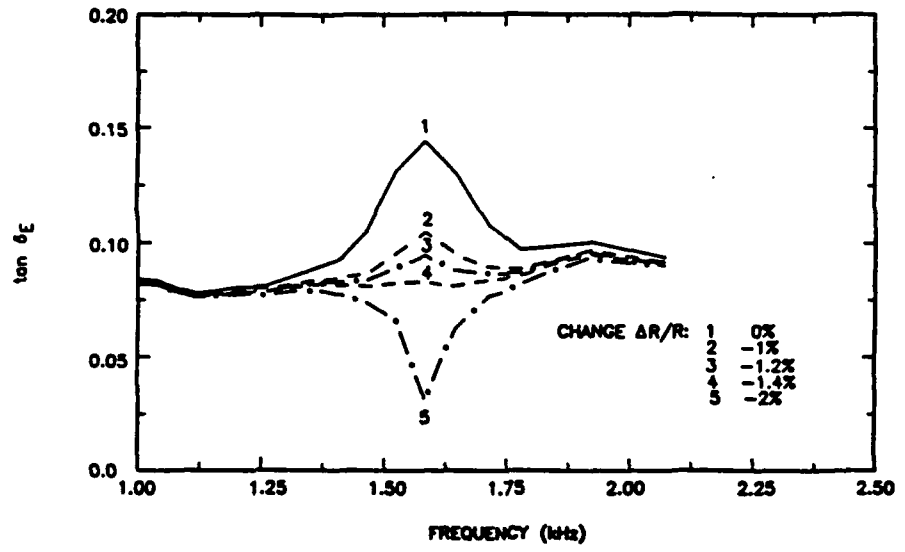

Fig. 13. Effect of applying various percentage changes to the ratio R on the structure in tan δ_E near 1.6 kHz in Fig. 12

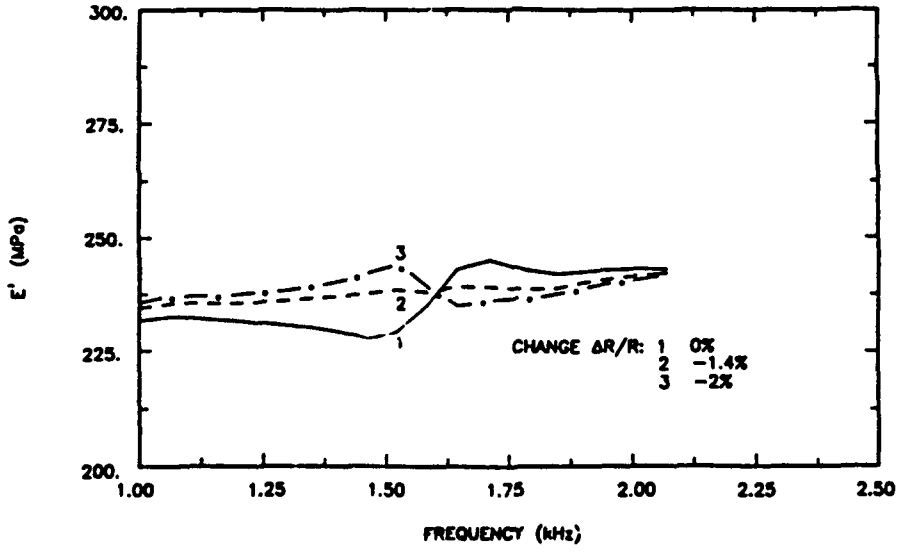

Fig. 14. Effect of applying various percentage changes to the ratio R on the structure in E' near 1.6 kHz in Fig. 9

In some cases, a systematic variation of E' at the low frequency end of the range was apparent, amenable to correction by means of a percentage change in the ratio R. Figure 15 shows an example for the alumer consisting of PR 1526 in a matrix of 6%, 40 ppi foamed aluminum. It appears that $\Delta R/R = -2\%$ gives the best result. This same percentage correction was applied throughout the whole frequency range, with some success at the first peak, but with little effect on the ones at higher frequency. The effect on tan δ_E is quite modest: the low frequency range is hardly affected, the first peak in the loss tangent data between 1 and 2 kHz appears to have been reduced, but the following peaks are again practically unaffected by this correction.

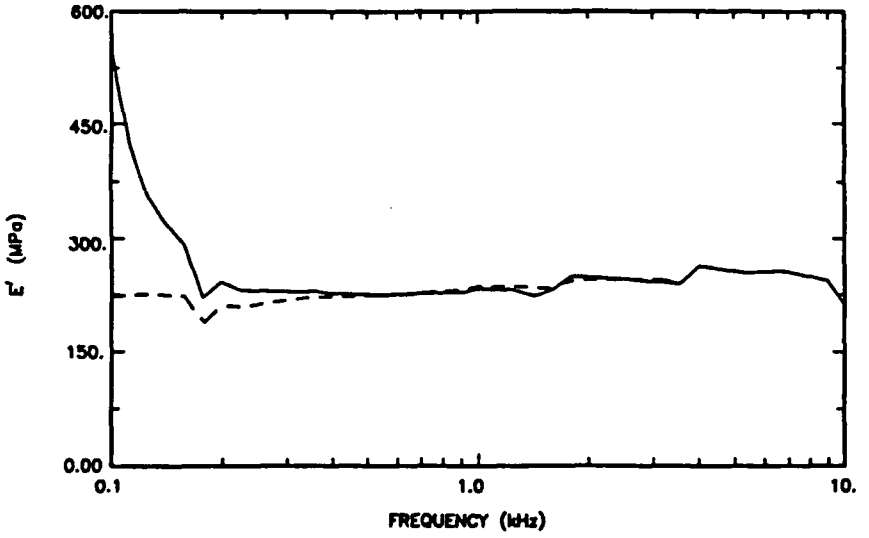

Fig. 15. Effect of applying a correction of -2% to the ratio R on the values of E' (from the data reduction) as a function of frequency. The sample is PR 1526 in 6%, 40 ppi foamed aluminum. Solid curve, uncorrected; dashed curve, corrected.

Before discussing possible causes for an error in R, the consequence of an error in the ratio $r = m_3/m_2$ is explored. Again, approximating the errors by the first term in a series expansion one finds that

$$\frac{\Delta z}{z} \simeq - \frac{r \sin z}{(1+r) \sin z + r z \cos z} \frac{\Delta r}{r}, \qquad (7)$$

where Δr is the error in r.

By a procedure similar to that leading to Fig.13, it was found that a percentage error of 2% in r provided the best correction at the first peak in $\tan \delta_E$. It is remarkable that the shape of the correction curve at higher frequencies was very similar to that computed from an assumed error in R; thus, experimentally one cannot decide between a constant error in r or in R as the cause of the structure. Of course, a better than 2% accuracy in the measurement of the masses of tip and sample is easily obtained, which makes an error in r a less probable cause for the observed structure than an error in R.

A relative error in the measured length of the bar translates directly into an equal relative error in $z = k\ell$, without any amplification.

An error in the ratio R may have various causes. First, it may be due to an error in the calibration of the accelerometers; even introducing the corrections to the nominal sensitivities, as a function of selected frequencies (provided by the manufacturer), may not be sufficiently precise. In the second place, it is quite possible that the lack of rigidity in the attachment of the bar to tip and base could cause an error, which, when amplified by the above effect, adds to the observed structure.

To investigate this source of error, a model was developed for the wax connections at the base and tip of the bar, described in Appendix B. With thicknesses of 1 mm of wax at both tip and bar or either one separately, errors in R were derived of about the right order of magnitude. In Figs. 16 and 17 the value of the relative error in R is shown as caused by a 1 mm layer of wax at the tip and base, or on either surface separately. The values for the dynamic Young's modulus as measured at NRL-USRD were: $E' = 1.39$ GPa, $\tan \delta_E = 0.015$, and $\rho = 1520$ kg/m^3.

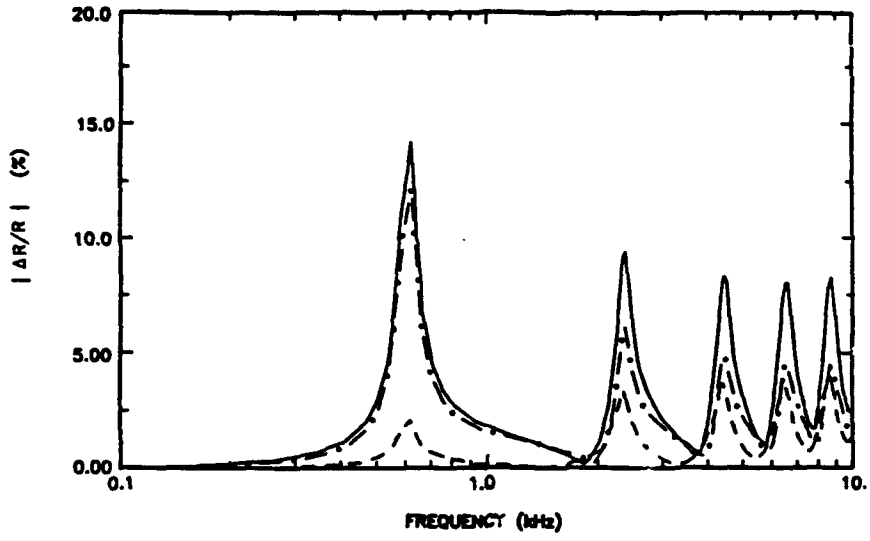

Fig. 16. Magnitude of the relative error in the ratio R, $|\Delta R/R|$, computed from model for wax connections at the base (thickness d_b) and tip (thickness d_t) of the sample bar. Solid curve, d_b = 1 mm, d_t = 1 mm; dashed curve, d_b=1 mm, d_t = 0 mm; dotted-dashed curve, d_b = 0 mm, d_t = 1 mm.

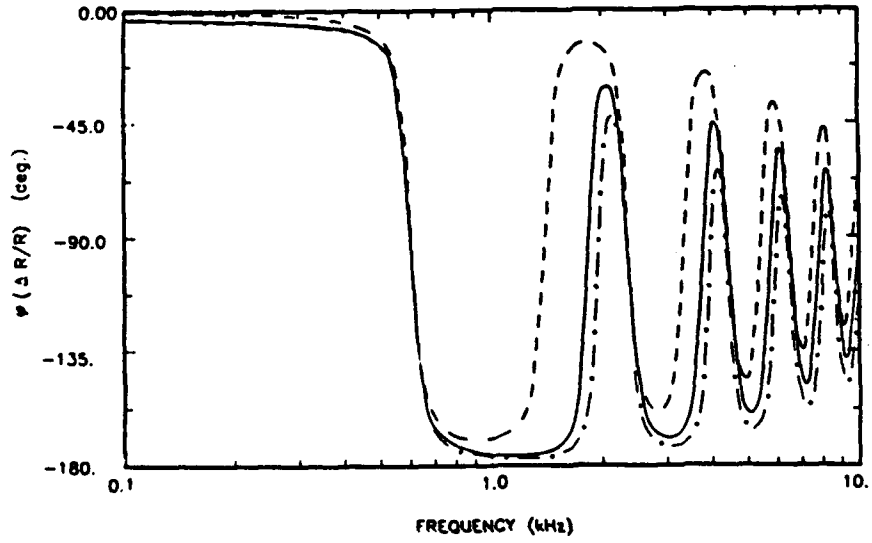

Fig. 17. Phase of the relative error in the ratio R, $\phi(\Delta R/R)$, computed from model for wax connections at the base (thickness d_b) and tip (thickness d_t) of the sample bar. Solid curve, d_b = 1 mm, d_t = 1 mm; dashed curve, d_b = 1 mm, d_t = 0 mm; dotted-dashed curve, d_b = 0 mm, d_t = 1 mm.

The absolute value of the relative error due to the wax reaches values up to 15%. It is remarkable, though, that the curves for the relative error in E' (Fig. 18) and the error in tan δ (Fig. 19), found by applying the correction due to the wax, are very similar to those for constant $\Delta R/R$ or $\Delta r/r$. They show that the corrections for E' and tan δ_E at the first structure are of the right order of magnitude, but they are not sufficient to explain the higher frequency peaks.

The conclusion to be drawn from this error analysis is that the method of measuring the dynamic Young's modulus is suitable for reaching considerable precision, on the order of one percent, even in the frequency range well away from the antiresonances. In the first place, it is necessary that the sensitivity of the accelerometers is sufficiently well known. It would be possible, in principle, to eliminate the effect of inaccuracy in the sensitivity of the accelerometers by measuring the ratio R_1 with accelerometers 1 and 2 (sensitivities s_1 and s_2) attached to tip and base respectively, and then finding R_2 after the two accelerometers were switched. Given the accelerations a_1 and a_2 of tip and base, one finds that $R_1 = s_2a_2/s_1a_1$ and $R_2 = s_1a_2/s_2a_1$. The desired ratio of accelerations of base and tip would be given by $R = \sqrt{(R_1R_2)}$. This has not been tried in practice. In the csecond place, it may be necessary to account for the wax connections at tip and base. It is possible, of course, that other sources of error exist that mimic the effect of the error sources discussed above. (One might think of effects due to the discontinuities in the bar at the tip and base, resulting in effects not described in the one-dimensional theory.) Moreover, errors from more than one source may be present simultaneously.

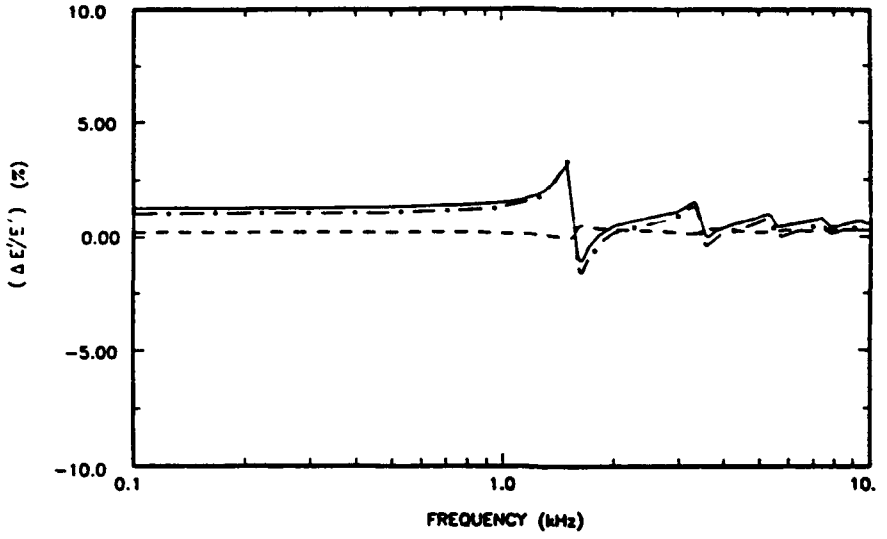

Fig. 18. Relative error in the real part of Young's modulus $\Delta E'/E'$ computed from model for wax connections at the base (thickness d_b) and tip (thickness d_t) of the sample bar. Solid curve, d_b = 1 mm, d_t = 1 mm; dashed curve, d_b = 1 mm, d_t = 8 mm; dotted-dashed curve, d_b = 8 mm, d_t = 1 mm.

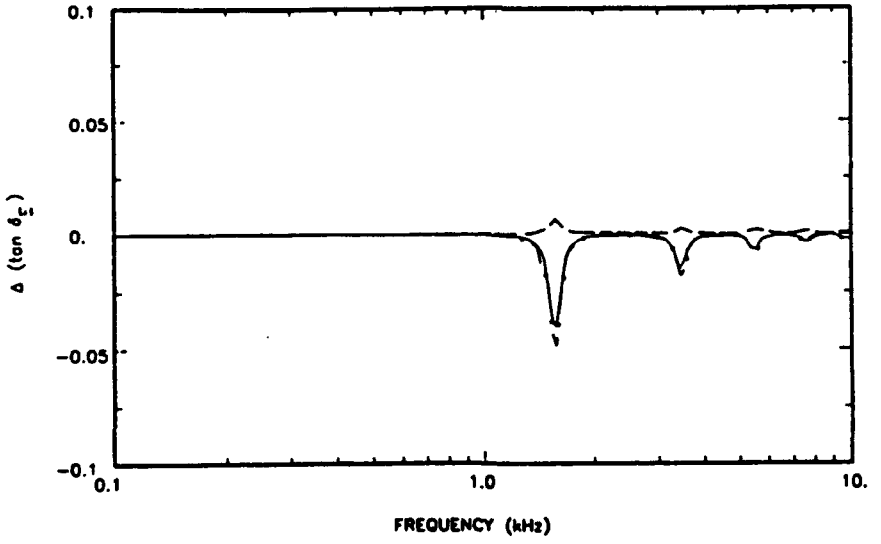

Fig. 19. Error in the loss tangent $\Delta(\tan \delta_E)$, computed from model for wax connections at the base (thickness d_b) and tip (thickness d_t) of the sample bar. Solid curve, d_b = 1 mm, d_t = 1 mm; dashed curve, d_b = 1 mm, d_t = 8 mm; dotted-dashed curve, d_b = 8 mm, d_t = 1 mm.

It would seem to be a valid interpolation to correct the observed ratio R by a constant percentage error for each of the ranges between two successive antiresonances. This interpolation has not been performed in the present study, except for the above examples. Since the main purpose of this study was to examine the behavior of various combinations of the constituents in a composite alumer, the representative values of E' and tan δ_E have been taken at a fixed frequency of 708 Hz (this frequency was a measurement point), where the deviation due to uncertainty in R is small. In general, this is close to the location of the first antiresonance. The frequency of the first antiresonance is given in Tables 4a through 4d.

In Ref. 10 it was reported that the Young's modulus measurement as a function of frequency for foamed aluminum showed a negative trend. This slope could be reduced to zero by introducing a small percentage shift in R. Since the velocities of tip and base were measured by laser Doppler, the error cannot be due to accelerometers in this case.

The choice of the ratio $r = m_3/m_2$ is mainly determined by the lower frequency limit that one wants to attain. For instance, with the values for the parameters given above and a 1% error in R, a 1% error in E' will be found at a frequency of 407 Hz with the ratio r = 1. For a ratio of r = 0.1, this one percent error in E' is found at a frequency of 665 Hz; for r = 10, the frequency limit for errors in E' below 1% decreases to 149 Hz.

RESULTS FOR YOUNG'S MODULUS

In Table 4 the results for the real part of Young's modulus E' and its loss tangent tan δ_E are collected. Table 4 has four parts (a, b, c, and d) for the four polyurethanes PR 1526, PR 1538, PR 1574, and PR 1590, respectively. In each case the data for the pure polymer are given first, computed from the polynomial coefficients in Ref. 7, followed by the Young's moduli for the foamed aluminum taken from Ref. 10.

Table 4 - Values of Young's modulus for polyurethanes, foamed aluminum and alumers. The values for the real part E' and loss tangent tan δ_E are given for a frequency of 708 Hz. The lowest antiresonance frequency f_{ar} is stated where applicable, to an accuracy determined by the sampling density. Unless otherwise indicated, the temperature is about 22°C. The data for the polyurethanes are from Ref. 9; the foamed aluminum data from Ref. 6. There are four parts on separate pages: 4a - PR 1526; 4b - PR 1538; 4c - PR 1574; 4d - PR 1590.

Legend (for all four parts):

Tip	nominal cross section of bar and tip	mass of tip, (incl. accelerom.)
S - Short steel	3/4x3/4 in^2	19.7 g
T - Thick steel	3/4x3/4 in^2	37.2 g
A - Short alum.	3/4x3/4 in^2	8.7 g
SS - Short steel	9/16x9/16 in^2	11.8 g
ST - Thick steel	9/16x9/16 in^2	21.4 g
SA - Short alum.	9/16x9/16 in^2	5.5 g

Standard length bar is about 11.3 cm (4.5 in.)
Long - Long bar, about 14.9 cm (5 7/8 in.)

4a

Conditions	Date	E' (MPa)	tan δ_E	f_{ar} (Hz)
PR 1526, ρ=1000 kg/m^3, Foamed aluminum, 6%, 10 ppi		16.7 207	0.60	
Alumer	4/24/91	224.6	0.094	562
	4/29/91	212.2	0.076	562
	Average	219	0.085	

4a (Continued)				
Conditions	Date	E_1 (MPa)	tan δ_E	f_{ar} (Hz)
Foamed aluminum, 6%, 20 ppi		194 or 157		
Alumer	4/19/91	288.4	0.061	631
	4/22/91	301.8	0.079	699
	7/02/91	284.8	0.066	643
	Average	292	0.069	
Foamed aluminum, 6%, 40 ppi		174		
Alumer	4/12/91	244.7	0.112	597
	4/19/91	237.7	0.106	562
	5/01/91	226.9	0.098	562
	Average	236	0.11	
Foamed aluminum, 12%, 10 ppi		236		
Alumer; A	8/06/91	269.2	0.082	926
S	8/01/91	273.2	0.080	794
S	8/02/91	274.6	0.081	794
T	7/31/91	269.9	0.082	656
	Average	272	0.081	
Foamed aluminum, 12%, 20 ppi		311		
Alumer; A	8/08/91	329.2	0.065	1020
S	8/12/91	331.0	0.066	858
T	8/13/91	334.7	0.070	708
	Average	332	0.067	
Foamed aluminum, 12%, 40 ppi		251		
Alumer; A	8/26/91	462.7	0.073	1166
S	8/14/91	477.9	0.075	1000
T	8/13/91	484.4	0.073	825
	Average	475	0.074	
S; 19°C	8/21/91	499.6	0.085	1020
S; 21°C	8/19/91	486.7	0.079	1000
S; 27°C	8/20/91	465.2	0.067	981

4b				
Conditions	Date	E' (MPa)	tan δ_E	f_{ar} (Hz)
PR 1538, ρ=1120 kg/m^3,		43.7	0.29	
Foamed aluminum, 6%, 10 ppi		207		
Alumer	1/25/91	172.3	0.143	502
	2/06/91	173.0	0.133	532
	2/08/91	183.7	0.162	562
	2/27/91	181.3	0.123	532
	7/19/91	187.7	0.120	532
A	7/25/91	189.2	0.122	810
S	7/24/91	189.0	0.122	668
T	7/30/91	191.4	0.128	552
Long, A	7/24/91	202.5	0.113	573
Long, S	7/23/91	206.6	0.109	502
SA	9/10/91	176.9	0.150	750
SS	9/09/91	174.9	0.139	631
ST	9/06/91	178.2	0.142	501
Long, SA	10/01/91	173.9	0.148	573
Long, SS	10/03/91	165.9	0.150	492
Long, ST	10.04/91	165.4	0.157	414
	Average	181	0.136	
Long, S	7/17/91	233.8	0.103	447
Long, S	7/17/91	231.7	0.099	438
SA, 21°C	9/16/91	177.8	0.151	750
SA, 26°C	9/18/91	163.3	0.137	722
Foamed aluminum, 6%, 20 ppi		194 or 157		
Alumer	1/31/91	295.7	0.071	667
	2/04/91	300.9	0.088	708
	2/06/91	302.4	0.082	708
	2/27/91	297.5	0.079	667
	Average	299	0.080	
SA, 23°C	12/04/91	241.9	0.075	858
SS, 23°C	12/06/91	252.6	0.084	736
Foamed aluminum, 6%, 40 ppi		174		
Alumer	1/28/91	234.2	0.109	631
	1/30/91	230.0	0.084	631
	1/30/91	238.0	0.096	631
	2/08/91	225.9	0.093	708
	2/25/91	227.3	0.105	708
	10/25/91	236.6	0.102	750
SA	10/25/91	221.8	0.106	825
SS	10/23/91	222.4	0.106	695
ST	10/28/91	219.0	0.106	584
	Average	228	0.100	
ST, 20°C	11/25/91	233.0	0.108	607

4c				
Conditions	Date	E' (MPa)	tan δ_E	f_{ar} (Hz)
PR 1574, ρ=1000 kg/m^3		203	0.12	
Foamed aluminum, 6%, 10 ppi		207		
Alumer	5/09/91	563.5	0.047	909
	5/16/91	564.6	0.046	891
	6/03/91	559.6	0.056	891
	6/17/91	580.5	0.050	891
	6/20/91	586.5	0.058	891
	Average	571	0.051	
SS, 23°C	12/20/91	472.4	0.052	1039
Foamed aluminum, 6%, 20 ppi		194 or 157		
Alumer	5/06/91	666.0	0.032	1000.
	5/31/91	633.9	0.049	1000.
	Average	650	0.041	
Foamed aluminum, 6%, 40 ppi		174		
Alumer	5/05/91	566.9	0.047	891
	6/03/91	555.0	0.055	891
	Average	561	0.051	

4d				
Conditions	Date	E' (MPa)	tan δ_E	f_{ar} (Hz)
PR 1590, ρ=1100 kg/m^3		42.4	0.41	
Foamed aluminum, 6%, 10 ppi		207		
Alumer	3/01/91	215.8	0.106	562
	3/20/91	230.4	0.110	562
	3/29/91	233.4	0.119	562
	4/01/91	226.3	0.101	562
	6/24/91	227.6	0.103	584
	Average	227	0.108	
SA 21.5°C	11/07/91	203.7	0.132	779
ST 21.5°C	11/07/91	203.3	0.132	562
	Average	199	0.140	
SS 22.0°C	11/01/91	190.3	0.157	631
Foamed aluminum, 6%, 20 ppi		194 or 157		
Alumer	3/01/91	316.4	0.082	708
	3/18/91	318.7	0.079	708
SA 21.5°C	11/05/91	322.4	0.099	962
SS 21.5°C	11/04/91	319.0	0.096	810
ST 21.5°C	11/05/91	319.8	0.108	681
	Average	319	0.093	
Foamed aluminum, 6%, 40 ppi		174		
Alumer	3/01/91	258.0	0.113	631
	3/18/91	248.2	0.120	631
ST 22°C	10/29/91	245.4	0.126	610
	Average	250	0.120	
SA 21.5°C	11/08/91	275.3	0.122	910
SS 21.5°C	11/12/91	283.2	0.128	779
ST 21.5°C	11/13/91	279.4	0.127	644
	Average	279	0.126	

The legend for Table 4 shows the various values of the parameters used in the experiments. Most of the measurements are done for a standard bar, with nominal length of 11.4 cm (4.5 in.); whenever a long bar was used this is indicated by "long," its nominal length is 14.9 cm (5 7/8 in.). The parameters were varied in order to check the validity of the experiments: the values for E' and tan δ_E should be independent of the choice of parameters. This is true in most situations and is discussed further below.

By scanning the values in Table 4, one may obtain a feeling for the spread in the data. The values for Young's modulus are given for the same frequency (708 Hz), where the structure referred to in an earlier section is of little influence. For general information, the lowest frequency is given where the absolute value of the tip-to-base voltage ratio is maximum. This is close to the first antiresonance of the bar-tip system. The accuracy of this value is dependent on the sampling density used.

As the simplest of models to combine moduli of constituents, one may consider the two extremes of a series or a parallel combination. Assuming that in the alumer the displacement of the two constituent solids is the same, while the applied force is distributed, one could opt for an addition of the Young's moduli of the constituents to obtain the modulus of the composite, for a first crude insight into the measurement results.

The following features in the data deserve attention:

1. Table 4a. For the alumers based on polyurethane PR 1526, the 6%, 10 ppi type has an E' that is about equal to the sum of the moduli for the foamed aluminum and the pure polymer. The value is slightly larger for the 40 ppi type, but the value of E' is considerably larger than this sum for the 20 ppi type. This points out that the pore size of the aluminum matrix has a noticeable influence in addition to its porosity, contrary to the assumption in the various models, which ignore the pore size effect. The influence of pore size is confirmed in all the other data presented. This point is brought to the fore by the 12% relative density foam: here the 20 ppi type shows little difference in the E' value between foam and alumer, while the 40 ppi type displays considerable difference. Notice that the pore size of the foamed

aluminum depends on the relative density, in addition to the pores-per-inch designation; for a higher density foam, the wall thickness is larger and thus the pore size is smaller. The loss tangent does not display any sizable differences from one type of alumer to the next, but it is much smaller than the loss tangent of the pure elastomer, which is near 0.6.

The spread in the results for different tip masses is well within the error limits. The measurements at different temperatures for the 12%, 40 ppi type show a decrease for increasing temperature, as would be expected for a viscoelastic material; the steps appear larger, though, than those for the pure polymer at the same temperatures.

2. Table 4b. With alumers based on the PR 1538 elastomer, this table shows a reasonable agreement between the results for the 6%, 10 ppi type. Only the two measurements for a long bar with regular cross section (Long, S) are somewhat outside the expected range of error, for unknown reasons. The 20 ppi type again has an E' that is considerably larger than for the other two types, 10 ppi and 40 ppi. The temperature variation is as expected. The consistency of the 40 ppi data for various tip masses at small cross section (SA, SS, ST) is good. The loss tangent for the composite is again considerably smaller than that of the pure elastomer.

3. Table 4c. The polymer PR 1574 is much more rigid than the other three; this apparently leads to a large modulus for the alumer, larger even than the sum of the moduli of the constituents. The 20 ppi type again stands out by its larger E' as compared with the 10 ppi and 40 ppi types. The loss tangent shows little variation between the alumers; its value is less than one half of that of the pure polyurethane.

4. Table 4d. For the alumers based on PR 1590, one finds again that the 20 ppi type has a larger E' than the other types. The loss tangent is three to four times smaller than that of the pure elastomer. For the SA, SS and ST measurements of the 10 ppi type, at various temperatures, the values are contrary to what follows from viscoelastic behavior: the value at 21.5°C is smaller than at 22°C, although not by much. The cause of these deviations is unknown. The variations due to temperature in the 20 ppi type are within the

limits of error; for the 40 ppi type the effect of 0.5° difference in temperature is quite noticeable and has the correct sign; the lower temperature results in a larger E'.

DILATATIONAL WAVE SPEED IN ALUMERS

Table 5 shows various properties of alumers and the polyurethanes on which they are based. The bulk modulus is taken from Table 1, with interpolation of the temperature variation to approximate the value at 22°C. Young's modulus for the pure polyurethanes is computed from the polynomial coefficients in Ref. 7. Young's modulus for the alumers is taken from Table 4.

For application as an acoustically transparent material, the dilatational wave speed c_d, in addition to the density ρ, is important. The lowest wave speed is found for the PR 1538, 6%, 20 ppi alumer (Table 5). Its density is greater than that of the PR 1526 types, and thus the three types of alumer based on the PR 1526 polymer have the lowest ρc-product, close to 1.7 SI Mrayl. This value is only 3% smaller than the ρc-values for the PR 1538 alumers. The non-dimensional loss coefficient α/k' varies by about a factor of three in the set of alumers; it is smallest, 0.0033, for the PR 1574, 6%, 20 ppi type and largest, 0.010, for the PR 1590, 6%, 40 ppi type.

Table 5. Various computed elastic properties of polyurethanes and alumers at 20°C.

ρ-density; G'-real part of shear modulus; ν',ν''-real and imaginary part of Poisson's ratio; c_d, α/k'-wave speed and non-dimensional loss coefficient of dilatational waves; the complex wave number is $k^* = k' - i\alpha$; $(\rho c_d)_{rel}$ - ρc product relative to seawater with ρc = 1.539 SI Mrayl.

Material	ρ kg/m3	G' MPa	ν'	$-\nu''/\nu'$	c_d m/s	α/k'	ρc_d,SI Mrayl	ρc_d rel
Polymer PR 1526	1000	5.57	0.4988	0.0014	1525	0.0059	1.525	0.991
Alumer 10 ppi	1068	73.7	0.4814	0.0020	1584	0.0088	1.691	1.099
6% 20 ppi	1070	98.5	0.4814	0.0022	1608	0.0078	1.718	1.116
40 ppi	1057	79.4	0.4851	0.0031	1702	0.0069	1.702	1.106
Polymer PR 1538	1120	14.6	0.4969	0.0018	1455.	0.0042	1.630	1.059
Alumer 10 ppi	1121	60.8	0.4886	0.0029	1558	0.0069	1.746	1.135
6% 20 ppi	1152	101.	0.4804	0.0028	1526	0.0097	1.758	1.142
40 ppi	1134	76.7	0.4853	0.0029	1540	0.0078	1.746	1.135
Polymer PR 1574	1000	68.3	0.4866	0.0031	1616	0.0055	1.616	1.050
Alumer 10 ppi	1093	195.	0.4673	0.0033	1704	0.0040	1.863	1.211
6% 20 ppi	1098	222.	0.4631	0.0030	1716	0.0033	1.884	1.224
40 ppi	1086	191.	0.4683	0.0028	1718	0.0062	1.866	1.212
Polymer PR 1590	1100	14.2	0.4971	0.0023	1497	0.0065	1.647	1.070
Alumer 10 ppi	1169	76.4	0.4859	0.0027	1543	0.0092	1.804	1.172
6% 20 ppi	1160	108.	0.4805	0.0032	1572	0.0085	1.824	1.185
40 ppi	1180	81.2	0.4846	0.0033	1548	0.0101	1.826	1.186

CONCLUSIONS

- The bulk modulus of a given alumer is larger than the bulk modulus of the polyurethane used as a filler by slightly more than the relative density of the foamed aluminum matrix. (This rule is observed for the 6% aluminum type only.)

- The data set is insufficiently large and the available models inadequate to reliably predict the Young's modulus of new combinations. Systematic effects were found that point to the importance of the pore size in determining Young's modulus of the alumer.

- The loss tangent of Young's modulus of an alumer is generally much smaller than the loss tangent of the constituent pure polymer.

- The ρc-values for the alumers studied vary from 1.69 to 1.87 SI Mrayl.

- A preliminary study of possible sources of error in the measurement of the dynamic Young's modulus suggests that a high precision may be attained.

ACKNOWLEDGEMENTS

The author wishes to express his gratitude to Ms. M.Q. Samuels for the measurement of the viscoelastic properties of the wax used in the experiments. He also wishes to thank Mr. Benjamin J. Cole and Mr. Forrest M. Eggleston for their dedicated assistance in performing the measurements, reducing the data, and organising the results. This study was supported by the Office of Naval Research.

REFERENCES

1. C.M. Thompson, "Development of a structurally rigid, acoustically transparent plastic," *J. Acous. Soc. Am.* 83, 1138-1143 (1990).

2. P.S. Dubbelday and F.M. Eggleston, "Alumer: A 'rigid', acoustically transparent, composite material," *J. Acous. Soc. Am.* 89, 1867 (1991).

3. P.S. Dubbelday and K.M. Rittenmyer, "Shear modulus effect on acoustically transparent materials," *IEEE J. Oceanic Eng.* OE-12, 333-338 (1987).

4. J. Burns and P.S. Dubbelday, "Dynamic bulk modulus of various elastomers," *J. Polym. Sci., Polym. Phys. Ed.* 128, 1187-1205 (1990).

5. P.S. Dubbelday and J. Burns, "Dynamic bulk modulus of soft elastomers," *J. Wave-Material Interaction* 5 and 6, 181-210 (1991).

6. R.W. Timme, "Speed of sound in castor oil," *J. Acous. Soc. Am.* 52, 989-992 (1972).

7. R.N. Capps, Elastomeric Materials for Acoustical Applications (Naval Research Laboratory, Washington, D.C., 1989).

8. C. van der Poel, "On the rheology of concentrated dispersions," *Rheol. Acta* 1, 198-205 (1958).

9. R.M. Christensen, Mechanics of Composite Materials (Wiley, New York, 1979), p 51.

10. P.S. Dubbelday, "Poisson's ratio of foamed aluminum determined by laser Doppler vibrometry," *J. Acous. Soc. Am.* 91, 1737-1744 (1992).

11. P.S. Dubbelday, "Application of a new complex root-finding technique to the dispersion relations for elastic waves in a fluid-loaded plate," *SIAM J. Appl. Math.* 43, 1127-1139 (1983).

12. E.A. Friis, R.S. Lakes, and J.B. Park, "Negative Poisson's ratio polymeric and metallic foams," *J. Mater. Sci.* 23, 4406-4414 (1988).

13. W.E. Warren and A.M. Kraynik, "The linear elastic properties of open-cell foams," *J. Appl. Mech.* 55, 341-346 (1988).

14. T. Pritz, "Transfer function method for investigating the complex modulus of acoustic materials: rod-like specimen," *J. Sound Vib.* 81, sect. 3 (1982).

15. B.A. Auld, Acoustic Fields and Waves in Solids (Wiley, New York, 1973) Vol I, pp.362-364.

BLANK PAGE

Appendix A

STIFFNESS AND COMPLIANCE MATRICES

The following compliance and stiffness matrix relations apply to a system with one rotational symmetry axis [15], which is identical to the hexagonal system. The symmetry axis is indicated by the subscript 3.

The elastic compliance matrix is:

$$[s] = \begin{bmatrix} s_{11} & s_{12} & s_{13} & 0 & 0 & 0 \\ s_{12} & s_{11} & s_{13} & 0 & 0 & 0 \\ s_{13} & s_{13} & s_{33} & 0 & 0 & 0 \\ 0 & 0 & 0 & s_{44} & 0 & 0 \\ 0 & 0 & 0 & 0 & s_{44} & 0 \\ 0 & 0 & 0 & 0 & 0 & s_{44} \end{bmatrix}, \qquad \text{(A1)}$$

with $s_{66} = 2\ (s_{11}-s_{12})$.

The stiffness matrix [c] has the same form as the matrix [s], but here $c_{66} = 0.5\ (c_{11}-c_{12})$.

Relations between elements of the stiffness matrix [s] and the compliance matrix [s] are

$$\begin{aligned} c_{11} + c_{12} &= \frac{s_{33}}{s} \\ c_{11} - c_{12} &= \frac{1}{s_{11}-s_{12}} \\ c_{13} &= \frac{-s_{13}}{s} \\ c_{33} &= \frac{s_{11}+s_{12}}{s} \\ c_{44} &= \frac{1}{s_{44}}, \end{aligned} \qquad \text{(A2)}$$

with $s = s_{33}\ (s_{11}+s_{12}) - 2\ s_{13}^{2}$.

BLANK PAGE

Appendix B

MATHEMATICAL MODEL FOR EFFECT OF WAX CONNECTIONS

In this Appendix corrections are derived for the ratio of accelerations of base and tip of the sample bar, due to the lack of rigidity of the wax connections.

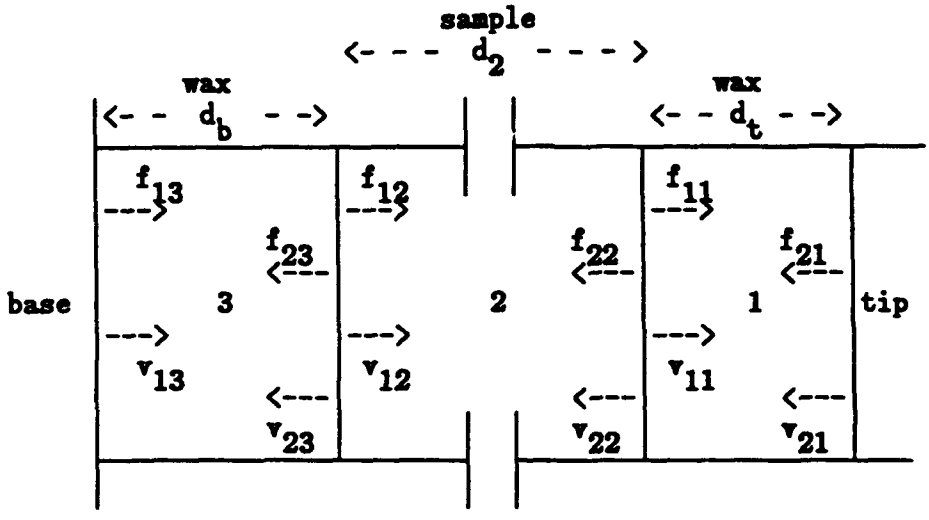

Fig. B1. Sketch of bar with wax connections and dynamic parameters

Figure B1 shows the basic features and definitions of some parameters of the model. A bar sample is attached by two wax layers to the tip and base. From linear waveguide theory one obtains the equations for the forces per unit area f_{ij} and velocities v_{ij} at the interfaces in the form

$$f_{11} = y_{11} v_{11} + y_{12} v_{21} \quad \text{(B1)}$$

$$f_{21} = y_{12} v_{11} + y_{11} v_{21} \quad \text{(B2)}$$

$$f_{12} = z_{11} v_{12} + z_{12} v_{22} \quad \text{(B3)}$$

$$f_{22} = z_{12} v_{12} + z_{11} v_{22} \quad \text{(B4)}$$

$$f_{13} = x_{11} v_{13} + x_{12} v_{23} \quad \text{(B5)}$$

$$f_{23} = x_{12} v_{13} + x_{11} v_{23}, \quad \text{(B6)}$$

where $y_{11} = \rho_1 c_1 / (i \tan k_1 d_t)$ ρ_1 - density of wax

$y_{12} = \rho_1 c_1 / (i \sin k_1 d_t)$ c_1 - bar speed in wax

$z_{11} = \rho_2 c_2 / (i \tan k_2 d_2)$ ρ_2 - density of sample

$z_{12} = \rho_2 c_2 / (i \sin k_2 d_2)$ c_2 - bar speed in sample

$x_{11} = \rho_1 c_1 / (i \tan k_1 d_b)$ k_1 - wavenumber in wax

$x_{12} = \rho_1 c_1 / (i \sin k_1 d_b)$ k_2 - wavenumber in bar

d_t - thickness of wax at tip d_b - thickness of wax at base

d_2 - length of sample bar m_2 - mass of the sample bar

In Eq. (B2) one has, for a harmonic wave,

$$f_{21} = \frac{- i\omega m_3 v_{21}}{A} = -z_3 v_{21}, \tag{B7}$$

where ω is the angular frequency, m_3 the mass of the tip, and A the cross-sectional area. The forces and velocities at the two interfaces of the interfaces of the sample bar are simply related, and thus the original unknowns, six forces and six velocities, reduce to eight unknowns. Eq. (B7) reduces the number to seven. Equation (B5) is extraneous to the computation, and thus five homogeneous equations remain in six unknowns.

One may solve Eqs. (B1, B2, B3, B4, and B6) for, say, f_{11}, f_{12}, v_{11}, v_{13}, and v_{21} in terms of v_{12}.

The observed ratio R_o = v(base)/v(tip) = $- v_{13}/v_{21} = (-v_{12}/v_{21})\ (v_{13}/v_{12})$. R_o is related to the ratio used in the data reduction R_c by $R_c = R_o + \Delta R$, where

$$R_c = \frac{z_{11}+z_3}{z_{12}} = \cos k_2 d_2 - \left[\frac{m_3}{m_2}\right] k_2 d_2 \sin k_2 d_2. \tag{B8}$$

From the algebraic solution to the equations it follows that

$$\frac{-v_{12}}{v_{21}} = R_c + \frac{R_c(y_{11}-y_{12})}{y_{12}} + \frac{y_{11}^2 - y_{12}^2}{y_{12}\, z_{12}} + \left[\frac{z_{11}}{z_{12}}\right] \left[\frac{z_3}{y_{12}}\right] = R_c + q_1. \tag{B9}$$

Retaining terms of order $k_1 d_t$ and $k_1 d_b$, q_1 is approximated by

$$q_1 \simeq \frac{y_{11}^2 - y_{12}^2}{y_{12} z_{12}} + \left[\frac{z_{11}}{z_{12}}\right]\left[\frac{z_3}{y_{12}}\right]. \tag{B10}$$

Next, the solution gives the second factor in the form

$$\frac{v_{13}}{v_{12}} = \frac{x_{11}}{x_{12}} + \Delta, \tag{B11}$$

where the first term on the right-hand side is of order 1, and Δ is shorthand for a correction term, to be stated explicitly later.

Thus one may write:

$$\begin{aligned} R_o = \frac{v(\text{base})}{v(\text{tip})} = (R_c + q_1)\left[\frac{x_{11}}{x_{12}} + \Delta\right] = R_c + q_1 + \left[\frac{x_{11}}{x_{12}} - 1\right](R_c + q_1) \\ + \Delta\,(R_c + q_1) = R_c + q_1 + q_2. \end{aligned} \tag{B12}$$

The correction term q_2 is found from the algebra to be:

$$\begin{aligned} q_2 = \Delta\,(R_c + c_1) = \frac{(y_{11}/y_{12})(z_{11}^2 - z_{12}^2)}{x_{12}\, z_{12}} + \left[\frac{y_{11}}{y_{12}}\right]\left[\frac{z_{11}}{z_{12}}\right]\left[\frac{z_3}{x_{12}}\right] \\ + \frac{(z_{11}/z_{12})(y_{11}^2 - y_{12}^2)}{x_{12} y_{12}} + \frac{(z_3/z_{12})(z_{11}^2 - z_{12}^2)}{x_{12} y_{12}}. \end{aligned} \tag{B13}$$

Retaining only errors of order $k_1 d_t$ and $k_1 d_b$, q_2 is approximated by

$$q_2 \simeq \frac{z_{11}^2 - z_{12}^2}{x_{12}\, z_{12}} + \left[\frac{z_{11}}{z_{12}}\right]\left[\frac{z_3}{x_{12}}\right]. \tag{B14}$$

The correction term q_1 is similar in form to the correction term q_2; they represent errors due to the wax at the tip and base, respectively.

SIMPLIFIED EXPRESSIONS FOR CORRECTIONS

In the following derivations it will be assumed that $k_1 d_t$ and $k_1 d_b$ are much smaller than one, so that $\sin k_1 d_t \simeq k_1 d_t$ and $\sin k_1 d_b \simeq k_1 d_b$.

By inserting the definitions for the quantities y_{ij}, z_{ij}, and z_3, the first term in the expression for q_1 may be reduced to a simpler form as follows:

$$- \frac{y_{11}^2 - y_{12}^2}{y_{12}\, z_{12}} = \left[\frac{\rho_1 c_1}{\rho_2 c_2}\right] k_1 d_t \sin k_2 d_2 = \left[\frac{\rho_1}{\rho_2}\right] k_2 d_t \sin k_2 d_2, \tag{B15}$$

and the second term leads to

$$\begin{aligned} - \left[\frac{z_{11}}{z_{12}}\right]\left[\frac{z_3}{y_{12}}\right] &= \left[\frac{(m_3/A)\,\omega\, k_1 d_t}{(\rho_1 c_1)}\right] \cos k_2 d_2 = \left[\frac{m_3}{m_1}\right] (k_1 d_t)^2 \cos k_2 d_2 \\ &= \left[\frac{m_3}{m_2}\right]\left[\frac{E_2}{E_1}\right] k_2 d_t\, k_2 d_2 \cos k_2 d_2, \end{aligned} \tag{B16}$$

where E_1, E_2 are the Young's moduli of the wax and the sample, respectively.

In a similar fashion one may reduce the first term of the expression for q_2 as follows:

$$\begin{aligned} - \frac{z_{11}^2 - z_{12}^2}{x_{12} z_{12}} &= \left[\frac{\rho_2 c_2}{\rho_1 c_1}\right] k_1 d_b \sin k_2 d_2 = \left[\frac{\rho_2 c_2}{\rho_1 c_1}\right] k_2 \left[\frac{c_2}{c_1}\right] d_b \sin k_2 d_2 \\ &= \left[\frac{E_2}{E_1}\right] k_2 d_b \sin k_2 d_2, \end{aligned} \tag{B17}$$

and the second term of q_2 becomes

$$- \left[\frac{z_{11}}{z_{12}}\right]\left[\frac{z_3}{x_{12}}\right] = m_3\, \omega \left[\frac{k_1 d_b}{\rho_1 c_1}\right] \cos k_2 d_2 = \left[\frac{m_3}{m_2}\right]\left[\frac{E_2}{E_1}\right] k_2 d_b\, k_2 d_2 \cos k_2 d_2. \tag{B18}$$

The total correction ΔR is equal to $-(q_1+q_2)$, and thus

$$\Delta R = \left[\frac{m_3}{m_2}\right]\left[\frac{E_2}{E_1}\right] k_2(d_t+d_b)\, k_2 d_2 \cos k_2 d_2 + k_2\left[\left[\frac{E_2}{E_1}\right]d_b+\left[\frac{\rho_1}{\rho_2}\right]d_t\right] \sin k_2 d_2. \quad \text{(B19)}$$